...

Paul Kotyczka* and Bernhard Maschke

Discrete port-Hamiltonian formulation and numerical approximation for systems of two conservation laws

...

Abstract: We discuss the discrete formulation of systems of conservation laws in port-Hamiltonian form on dual chain complexes. Based on integral balance equations and topological information, this representation is exact and qualifies as a control model. The finite-dimensional approximation requires an energy discretization that yields discrete constitutive equations. We give (i) a brief overview of discrete modeling of conservation laws on n-complexes and (ii) extend existing results by allowing for mixed physical types of boundary inputs. This requires the construction of a primal and a dual complex based on the underlying staggered grids and the localization of the inputs on the system boundary. Finally, (iii) we discuss the properties of the resulting structure-preserving discretization scheme based on a consistency analysis for the 2D nonlinear shallow water equations.

Keywords: Conservation laws, port-Hamiltonian systems, discrete formulation, structure-preserving discretization, finite volumes

Classification: ...

*Corresponding Author: Paul Kotyczka: Univ Lyon, Université Claude Bernard Lyon 1, CNRS, LAGEP UMR 5007, 43 Boulevard du 11 Novembre 1918, 69622 Villeurbanne Cedex, France. He is on temporary leave from Technical University of Munich, Chair of Automatic Control (Prof. B. Lohmann). E-mail: kotyczka@tum.de
Bernhard Maschke: Univ Lyon, Université Claude Bernard Lyon 1, CNRS, LAGEP UMR 5007, 43 Boulevard du 11 Novembre 1918, 69622 Villeurbanne Cedex, France. E-mail: bernhard.maschke@univ-lyon1.fr

Zusammenfassung: Wir diskutieren die diskrete Beschreibung von Systemen von Erhaltungsgleichungen auf dualen Kettenkomplexen in Port-Hamiltonscher Form. Die Darstellung beruht auf den integralen Bilanzgleichungen und der Topologie der Diskretisierungsgitter. Sie ist exakt und eignet sich als Regelungsmodell. Die endlich-dimensionale Näherung erfordert eine Diskretisierung des Energiefunktionals, welche auf diskrete Konstitutivgleichungen führt. Wir geben (i) einen kurzen Überblick über die diskrete Modellierung von Erhaltungsgleichungen auf n-Komplexen. Die systematische Konstruktion der dualen Komplexe auf Grundlage versetzter Gitter und der Verortung der Randeingriffe erweitert (ii) bestehende Ergebnisse um die Abbildung verschiedenartiger physikalischer Randeingänge. Schließlich diskutieren wir (iii) am Beispiel der nichtlinearen 2D-Flachwassergleichungen und auf Basis einer Konsistenzanalyse die Eigenschaften des resultierenden strukturerhaltenden Diskretisierungsverfahrens.

Schlüsselwörter: Erhaltungsgleichungen, Port-Hamiltonsche Systeme, diskrete Formulierung, strukturerhaltende Diskretisierung, Finite Volumen.

1 Introduction

In a port-Hamiltonian (PH) system description, see Duindam et al. (2009) for an overview PH-based modeling and control, the *interconnection structure* (and the dissipative structure) is separated from the *constitutive equations*. The first describes the lossless exchange of power between different types of energy, different system parts and the exterior in terms of port variables, i. e. pairs of collocated, power-conjugated physical quantities. Constitutive or closure equations can be derived from the stored energy or another potential and determine the nature of the considered finite- or infinite-dimensional system (linear or

nonlinear, hyperbolic or parabolic, see e.g. Baaiu et al. (2009), Zwart et al. (2016)). Power ports as interfaces between system parts make the PH approach appealing for modeling, simulation and control of multiphysics, coupled systems, see Falaize and Hélie (2016) and Cardoso-Ribeiro et al. (2017) for two recent examples.

For the numerical treatment of infinite-dimensional PH systems, see e.g. Altmann and Schulze (2017) for the non-trivial example of the Navier-Stokes reactive flow, a spatial (and finally temporal) discretization is necessary. The range of existing methods that preserve the PH structure in the finite-dimensional approximate model runs from mixed finite element methods using simple approximation forms (Golo et al., 2004) or higher order shape functions (Farle et al., 2013) up to pseudo-spectral methods (Moulla et al., 2012; Vu et al., 2017).

The approach presented in Seslija et al. (2012), Seslija et al. (2014) employs the language of discrete exterior geometry to formulate an integral representation of two conservation laws on a simplicial triangulation and its dual. The discrete linear constitutive relations are obtained by use of a diagonal discrete Hodge operator. In van der Schaft and Maschke (2013) and van der Schaft and Maschke (2011), the PH formulation of conservation laws on graphs and k-complexes is discussed. Hiemstra et al. (2014) give an extensive overview over *geometric discretization* – yet without boundary ports – which is based on the purely *topological* description of the conservation laws on the one hand, and approximations of the field variables, which commute with (exterior) differentiation on the other hand. The latter *"guarantees that conservation and balance laws remain exactly satisfied in the discrete setting"* (p. 1456).

In the present paper, we refer mainly to the results in Seslija et al. (2012), Seslija et al. (2014) and extend them in the following directions. We derive discrete input-/output representations for systems of two conservation laws with *arbitrary* combinations of boundary inputs (in the sense of their physical quantity, or *causality* of the boundary port variables). To this end, we construct dual chain complexes, based on the relations of primal and dual discretization grid and the system boundary. We show by means of a nonlinear 2D example on rectangular grids that the numerical approximation of the flux functions (integral efforts) by a centered control volume scheme is consistent of order 2 in the interior, which extends the 1D result in Kotyczka (2016). The shifted grids require to assume values for different state variables along the boundary. We discuss exemplarily the errors due to an (in-)consistent assignment of these *ghost values*.

The paper is organized as follows. We briefly present the necessary preliminaries on PH systems, differential forms and chain complexes in Section 2. Section 3 contains as first result the (exact) discrete formulation of conservation laws with arbitrary boundary inputs, based on a concise construction of the primal and the dual grid/complex. In Section 4, we consider the numerical approximation of the constitutive equations, which is the bridge to classical finite volume (control volume) schemes. By means of the 2D example of the nonlinear shallow water equations, we discuss the consistency of the method, followed by a series of remarks. We conclude with a summary and perspectives for future work in Section 5.

2 Preliminaries

We summarize and explain some basic ideas on PH systems, conservation laws, differential forms and the notion of (co)chain complexes in order to keep the exposition in Sections 3 and 4 self-contained. For details on the different aspects of the PH system representation, we refer to Duindam et al. (2009), van der Schaft and Maschke (2002), van der Schaft and Maschke (2013) and van der Schaft and Maschke (2011). In Flanders (1963) and Chapter 7 of Arnold (1989), the reader finds a concise and illustrative introduction to differential forms, their integration on discrete objects, (co)chains and the complex property. We frequently refer to Seslija et al. (2012), Seslija et al. (2014), where modeling of conservation laws using the "discrete exterior geometry approach" has been presented for control inputs of *uniform* physical type, and without treating the numerical approximation, in particular for nonlinear systems.

2.1 Finite-dimensional PH systems

Definition 1. A dynamical system of the form

$$\dot{\boldsymbol{x}} = (\boldsymbol{J}(\boldsymbol{x}) - \boldsymbol{R}(\boldsymbol{x}))\nabla H(\boldsymbol{x}) + \boldsymbol{G}(\boldsymbol{x})\boldsymbol{u} \qquad (1a)$$
$$\boldsymbol{y} = \boldsymbol{G}^T(\boldsymbol{x})\nabla H(\boldsymbol{x}) + \boldsymbol{D}(\boldsymbol{x})\boldsymbol{u} \qquad (1b)$$

with state vector $\boldsymbol{x} \in \mathbb{R}^n$, in- and (collocated, power conjugated) outputs $\boldsymbol{u}, \boldsymbol{y} \in \mathbb{R}^m$, interconnection, damping and feedthrough matrices $\boldsymbol{J} = -\boldsymbol{J}^T$, $\boldsymbol{R} = \boldsymbol{R}^T \geq 0$ and $\boldsymbol{D} = -\boldsymbol{D}^T$ and an energy (or Hamiltonian) function $H : \mathbb{R}^n \to \mathbb{R}$, which is bounded from below, is called finite-dimensional port-Hamiltonian (PH) system.

From the structure of the equations and the definiteness properties, the power balance $\dot{H} \leq \boldsymbol{y}^T \boldsymbol{u}$, and hence passivity of the PH state representation, immediately follows. If $\boldsymbol{x}^*$ is an *isolated* minimum of H, the Hamiltonian

serves (at least locally) as a Lyapunov function for the stable equilibrium $\boldsymbol{x}^*$ of the unforced system. Defining pairs of *port variables* (vectors of *flows* and *efforts*) associated to energy storage ($\boldsymbol{f} := -\dot{\boldsymbol{x}}$, $\boldsymbol{e} := \nabla H(\boldsymbol{x})$), dissipation ($\boldsymbol{e}_R := -\boldsymbol{R}(\boldsymbol{x})\nabla H(\boldsymbol{x})$, $\boldsymbol{f}_R := \nabla H(\boldsymbol{x})$), and the interconnection with the environment ($\boldsymbol{u}$, $\boldsymbol{y}$), the state representation (1a), (1b) can be recast as

$$\begin{bmatrix} \boldsymbol{f} \\ \boldsymbol{f}_R \\ \boldsymbol{y} \end{bmatrix} = \begin{bmatrix} -\boldsymbol{J} & -\boldsymbol{I} & -\boldsymbol{G} \\ \boldsymbol{I} & 0 & 0 \\ \boldsymbol{G}^T & 0 & 0 \end{bmatrix} \begin{bmatrix} \boldsymbol{e} \\ \boldsymbol{e}_R \\ \boldsymbol{u} \end{bmatrix}, \qquad (2)$$

and the the power balance $\boldsymbol{e}^T\boldsymbol{f} + \boldsymbol{e}_R^T\boldsymbol{f}_R + \boldsymbol{u}^T\boldsymbol{y} = 0$ becomes evident. This relation between pairs of power-conjugated variables defines (as a formal representation of power continuity) a *Dirac structure*. The energy-based system description and power-preservation are the basic ingredients for the success of PH methods for modeling of multiphysics, coupled systems and energy-based control like *Control by Interconnection* or *IDA-PBC*, see e. g. Ortega et al. (2001), Ortega et al. (2002), Kotyczka (2013).

2.2 PH formulation of conservation laws

We recall how PH systems may be generalized to distributed parameter (infinite-dimensional) systems, more precisely, systems of conservation laws. Therefore, we briefly summarize some definitions of integral calculus defined on differential forms.

2.2.1 Differential forms

An essential characterization of (exterior) differential forms (of degree k, or k-forms) is given on page 1 of Flanders (1963) as "*things which occur under integral signs*". However, they are not merely "densities", but they have an *orientation*, i. e. they contain the information about the sense of integration. Typical examples from electromagnetism[1] in $\mathbb{R}^3$ are the electric field one-form $E_x dx + E_y dy + E_z dz$, the current density 2-form $J_x dy \wedge dz + J_y dz \wedge dx + J_z dx \wedge dy$ or the charge density 3-form $\rho\, dx \wedge dy \wedge dz$. In $\mathbb{R}^n$, the differentials $\{dx_1, \ldots, dx_n\}$ form the basis of differential one-forms. Higher order basis forms are constructed using the wedge (or exterior) product, which due to its skew-symmetry ($dx_i \wedge dx_j = -dx_j \wedge dx_i$, $i \neq j$, $dx_i \wedge dx_i = 0$) induces the orientation. The *exterior derivative* d is a unique differential operator which maps k-forms to $(k+1)$-forms.

Acting on a 0-form (a function)/1-form/2-form in $\mathbb{R}^3$, it corresponds to the grad/rot/div operations from vector calculus and allows to generalize the different integration formulas by the *generalized Stokes' theorem*[2].

Theorem 1. *Let ω be a differential k-form and Ω a $(k+1)$-dimensional, oriented and bounded open manifold with Lipschitz-continuous boundary $\partial\Omega$. Then*

$$\int_\Omega \mathrm{d}\omega = \int_{\partial\Omega} \mathrm{tr}\,\omega. \qquad (3)$$

The *trace operator* tr defines the restriction of the k-form ω to the boundary[3]. For convenience, the symbol tr is frequently omitted, i. e. $\int_{\partial\Omega} \omega := \int_{\partial\Omega} \mathrm{tr}\,\omega$.

2.2.2 Conservation laws

We consider (lossless) systems of two conservation laws on an n-dimensional open domain Ω with Lipschitz boundary $\partial\Omega$. An integral representation is given by

$$\frac{d}{dt}\int_\Omega \alpha_p + \int_{\partial\Omega} \beta_p = 0, \qquad \frac{d}{dt}\int_\Omega \alpha_q + \int_{\partial\Omega} \beta_q = 0. \qquad (4)$$

The differential forms α_p, α_q of degree p and q, respectively, represent the *conserved quantities* and β_p, β_q (differential forms of degree $p-1$ and $q-1$, respectively) denote the *flux functions*. The relation $p + q = n + 1$ holds, see van der Schaft and Maschke (2002). For the PH formulation, the fluxes are related to a *Hamiltonian functional* $H = \int_\Omega \mathcal{H}(\alpha_p, \alpha_q)$, where $\mathcal{H}$ is the Hamiltonian density n-form. Defining the *effort* (or co-state) variables e_p, e_q as its variational derivatives[4]

$$e_p = \delta_{\alpha_p} H, \quad e_q = \delta_{\alpha_q} H, \qquad (5)$$

the fluxes are set as

$$\begin{bmatrix} \beta_p \\ \beta_q \end{bmatrix} = \begin{bmatrix} 0 & (-1)^{pq+1} \\ 1 & 0 \end{bmatrix} \begin{bmatrix} e_p \\ e_q \end{bmatrix}. \qquad (6)$$

Applying Theorem 1 to both conservation laws in (4) on any domain included in Ω, and replacing the flux functions, leads to

$$\frac{\partial}{\partial t}\alpha_p = (-1)^{pq}\mathrm{d}e_q, \qquad \frac{\partial}{\partial t}\alpha_q = -\mathrm{d}e_p. \qquad (7)$$

---

[1] See e. g. the recent article Warnick and Russer (2014) for an illustrative introduction to Maxwell's equations in terms of differential forms, with an abundant list of references.

---

[2] In Arnold (1989), it is nicely called *Newton-Leibniz-Gauss-Green-Ostrogradskii-Stokes-Poincaré formula*.

[3] See e. g. Brezis (2011), Section 9.8, pp. 315-316, or Quarteroni and Valli (1994), Section 1.3, p. 10, on the introduction of the trace operator in terms of functional analysis. Arnold et al. (2010) give in Section 4.1 a definition for differential forms.

[4] For the definition in terms of differential forms, see Duindam et al. (2009), p. 232, Prop. 4.2.

The exponent pq takes into account the orientations of the differential forms. The definition of a *boundary port* (f_∂, e_∂) yields the following definition.

Definition 2. The differential formulation of a PH system of two conservation laws is given by

$$\begin{bmatrix} \frac{\partial}{\partial t}\alpha_p \\ \frac{\partial}{\partial t}\alpha_q \end{bmatrix} = \begin{bmatrix} 0 & (-1)^{pq}\mathrm{d} \\ -\mathrm{d} & 0 \end{bmatrix} \begin{bmatrix} e_p \\ e_q \end{bmatrix} \tag{8a}$$

$$\begin{bmatrix} f_\partial \\ e_\partial \end{bmatrix} = \begin{bmatrix} \mathrm{tr} & 0 \\ 0 & (-1)^p\mathrm{tr} \end{bmatrix} \begin{bmatrix} e_p \\ e_q \end{bmatrix} \tag{8b}$$

In accordance with the finite-dimensional case, the power balance, which results from the structure of the equations and the application of Stokes' theorem, becomes

$$\dot{H} = \int_\Omega \delta_{\alpha_p}H \wedge \dot{\alpha}_p + \delta_{\alpha_q}H \wedge \dot{\alpha}_q = \int_{\partial\Omega} f_\partial \wedge e_\partial. \tag{9}$$

Remark 1. Based on differential forms and Stokes' theorem, *Stokes-Dirac structures* can be defined as the infinite-dimensional counterpart of *Dirac structures*, see e.g. van der Schaft and Maschke (2002). However, as we adopt a discrete/integral modeling perspective, it is not necessary to make use of them in this article.

2.3 The primal n-complex

Systems of conservation laws may also be expressed directly in a finite-dimensional/discrete space, as it is done e.g. in van der Schaft and Maschke (2011), Seslija et al. (2012). To introduce the necessary notions for the integration of differential forms on *discrete* objects, we consider Fig. 1 which we will identify as the graphical representation of a 2-complex. The non-rectangular, *oriented* mesh could result from a polyhedral tessellation[5] K on a subset of $\mathbb{R}^2$. The mesh is based on five nodes $n_1, \ldots, n_5 \in \mathcal{N}$, connected by six oriented edges $e_1, \ldots, e_6 \in \mathcal{E}$ which divide the convex hull of the nodes into two oriented faces $f_1, f_2 \in \mathcal{F}$. The sets of nodes, edges and faces have cardinalities $|\mathcal{N}| = 5$, $|\mathcal{E}| = 6$, $|\mathcal{F}| = 2$.

Remark 2. We have arbitrarily defined the object in Fig. 1 to represent a mesh on $\mathbb{R}^2$. It could also display some "folded" two-dimensional manifold in $\mathbb{R}^3$. To know about the shape of the underlying object, the *topological* information must be completed by *geometric* data.
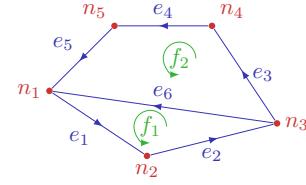
Fig. 1. A non-simplicial mesh in 2D, composed of oriented cells

2.3.1 j-cells, j-chains and j-cochains

We start with the definition of the most important discrete objects of a *chain complex*.

Definition 3 (Arnold (1989), p. 184). A j-*dimensional cell* or j-*cell* of an n-dimensional smooth manifold M is characterized by an oriented convex polyhedron $D \subset \mathbb{R}^j$, and a differentiable map[6] $f: D \to M$.

Nodes, edges and faces in Fig. 1 represent 0-cells, 1-cells and 2-cells, with orientations indicated by the arrows. The sets $\mathcal{N}, \mathcal{E}, \mathcal{F}$ (or subsets thereof) are the bases of j-*chains* ($j = 0, 1, 2$) according to the following definition.

Definition 4 (Arnold (1989), p. 185). A j-*dimensional chain* or j-*chain* is a finite-dimensional collection (or a formal sum) of j-cells σ_i, weighted by scalars (multiplicities) m_i: $c_j = m_1\sigma_1 + \ldots + m_r\sigma_r$. The linear vector space of j-chains on a tessellation K is denoted[7] $C_j(K; \mathbb{R})$.

According to the definition, the simplest j-chain is a j-cell. If the multiplicities are restricted to $\{-1, 0, 1\}$, a j-chain can be considered as the concatenation of several j-cells, e.g. the 1-chain $e_3 + e_4 + e_5 - e_6 =: \partial_2 f_2$, which forms the (oriented) boundary of the 2-cell f_2.

Definition 5 (Frankel (2011), p. 638). A j-*cochain* is a linear functional on the j-chains.

The linear functional on the j-chains can be understood via the *duality pairing* $\langle \cdot, \cdot \rangle : C^j(K; \mathbb{R}) \times C_j(K; \mathbb{R}) \to \mathbb{R}$, where $C^j(K; \mathbb{R})$ denotes the linear vector space of cochains. Hence, j-cochains $c^j \in C^j(K; \mathbb{R})$ are *algebraically*[8] dual objects with respect to this pairing. In our context, j-cochains will contain the integral values of j-forms on j-cells. Later on, we will define discrete state and

---

[6] This map is $f = \mathrm{id}$ if $M = \mathbb{R}^n$.

[7] $\mathbb{R}$ indicates that the multiplicities are real-valued.

[8] In contrast to topological duality based on which the dual grid/complex is constructed.

[5] To distinguish from a *simplicial triangulation* as in Seslija et al. (2014).

effort vectors which can be understood as vector-valued representations of such j-cochains.

2.3.2 Boundary maps and chain complex

Each j-cell has a *boundary* which is composed of $(j-1)$-cells whose orientation is *induced* by the orientation of the j-cell, see e.g. $\partial_2 f_2$ as defined above. The symbol ∂_j will at the same time denote the boundary map $\partial_j : C_j \rightarrow C_{j-1}$ and its matrix representation. Let $\hat{\imath}_k^{\mathcal{F}}$ ($\hat{\imath}_l^{\mathcal{E}}$) be a $|\mathcal{F}|$-dimensional ($|\mathcal{E}|$-dimensional) unit vector. Then $\partial_2 \hat{\imath}_k^{\mathcal{F}}$ ($\partial_1 \hat{\imath}_l^{\mathcal{E}}$) returns the $|\mathcal{E}|$-dimensional ($|\mathcal{N}|$-dimensional) vector with elements from $\{-1, 0, 1\}$ indicating the edges (nodes) that form the boundary of the 2-cell f_k (the 1-cell e_l). The *boundary* or *incidence*[9] *matrices* for the depicted example are

$$\partial_1 = \begin{bmatrix} -1 & 0 & 0 & 0 & 1 & 1 \\ 1 & -1 & 0 & 0 & 0 & 0 \\ 0 & 1 & -1 & 0 & 0 & -1 \\ 0 & 0 & 1 & -1 & 0 & 0 \\ 0 & 0 & 0 & 1 & -1 & 0 \end{bmatrix}, \quad \partial_2 = \begin{bmatrix} 1 & 0 \\ 1 & 0 \\ 0 & 1 \\ 0 & 1 \\ 0 & 1 \\ 1 & -1 \end{bmatrix}.$$

It is easy to verify at the example that $\partial_1 \circ \partial_2 = 0$, i.e. the range of ∂_2 spans the kernel of ∂_1. This property holds for any concatenation of two subsequent boundary maps: "*[T]he boundary of each chain itself has zero boundary*" (Flanders (1963), p. 59) and is known in general as the *complex property*. We can illustrate the relations between the spaces of j-chains and the boundary maps with $\partial_{j-1} \circ \partial_j = 0$, $j = 2, \ldots, n$, by the sequence diagram

$$C_n(K;\mathbb{R}) \xrightarrow{\partial_n} C_{n-1}(K;\mathbb{R}) \xrightarrow{\partial_{n-1}} \cdots \xrightarrow{\partial_1} C_0(K;\mathbb{R}). \tag{10}$$

Figure 1 represents such a *chain complex* for $n = 2$. By identifying the graphical representation with the object behind, we will for brevity refer to it as a 2-complex.

Remark 3. A *(chain) complex* is in a general manner defined as a sequence of abelian groups (e.g. vector spaces), connected by homomorphisms, i.e. mappings that preserve the group operation[10]. Famous examples are (i) the sequence of smooth function spaces, connected via the differential operations grad/rot/div and (ii) the so-called *de Rham* complex with spaces of (smooth) differential forms, connected via the exterior derivative d.

---

9 As in van der Schaft and Maschke (2011), we will use rather the terms (co-)incidence maps instead of (co-)boundary maps to distinguish from the boundary port variables.
10 See e.g. Jänich (2001), p. 127.
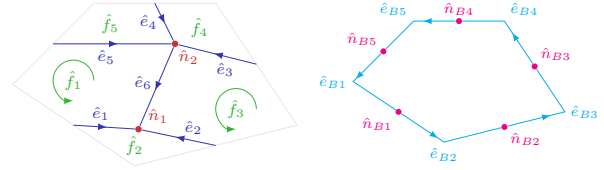
Fig. 2. The dual 2-complex and the dual boundary

2.3.3 Coboundary maps and cochain complex

Using the duality pairing between chains and cochains, the *coboundary operator* d^j can be defined via

$$\langle c^{j-1}, \partial_j c_j \rangle = \langle \mathrm{d}^j c^{j-1}, c_j \rangle, \tag{11}$$

which gives rise to the sequence diagram

$$C^0(K;\mathbb{R}) \xrightarrow{\mathrm{d}^1} C^1(K;\mathbb{R}) \xrightarrow{\mathrm{d}^2} \cdots \xrightarrow{\mathrm{d}^n} C^n(K;\mathbb{R}) \tag{12}$$

of the *cochain complex* with $\mathrm{d}^j \circ \mathrm{d}^{j-1} = 0$, $j = 2, \ldots, n$. Assuming the chain c_j represented by a column vector and the cochain c^{j-1} by a row vector, the relation between the matrix representations of boundary and coboundary map becomes evident:

$$\mathrm{d}^j = (\partial_j)^T. \tag{13}$$

Remark 4. The co-incidence operator d^j is the discrete counterpart of the exterior derivative, and therefore can be understood as *discrete exterior derivative* (Seslija et al., 2014). Accordingly, j-cochains in the discrete setting correspond naturally to j-forms and Eq. (11) can be considered the discrete version of Stokes' theorem.

2.3.4 Trace operators

The *trace operators* $\mathrm{tr}_j : C_j(K;\mathbb{R}) \rightarrow C_j(\partial K, \mathbb{R})$, $j = 0, \ldots, n-1$, isolate the j-chains on the boundary of the n-complex. For the example, and again identifying the operator with its matrix representation, we have

$$\mathrm{tr}_0 = I_5, \qquad \mathrm{tr}_1 = \begin{bmatrix} I_5 & 0_{5 \times 1} \end{bmatrix}. \tag{14}$$

2.4 The dual n-complex

To each j-cell on a n-complex, we can associate a *topologically* dual $(n-j)$-cell, which can have different *geometric* realizations (e.g. barycentric, circumcentric). In our 2D example, a node has a dual surrounding face, an edge has a dual edge across it, see Fig. 2, left. When we refer to "topological duality", which manifests itself in the relation of primal and dual (co-)incidence matrices, see below, we tacitly associate it with its geometric realization.

Relations of the co-incidence matrices

Between the co-incidence matrices of an n-complex and its dual, the following relation holds[11] (first formula in Section 3.3 of Seslija et al. (2014), in our notation)

$$\hat{d}^{n-j+1} = (-1)^j (d^j)^T. \tag{15}$$

In our example we have $\hat{d}^1 = (d^2)^T$ and $\hat{d}^2 = -(d^1)^T$. The construction of dual $(n–j)$-cells leaves out the boundary ∂K of the original complex, which is represented by a boundary $(n−1)$-chain. The dual n-complex is provided with a boundary $(n−1)$-chain (whose j-cells are indexed B) by topological duality on ∂K. With the second formula in Section 3.3 of Seslija et al. (2014) in our notation,

$$\hat{d}_B^{n-j} = (-1)^j (tr_j)^T, \tag{16}$$

we obtain in our example $\hat{d}_B^1 = -(tr_1)^T$ and $\hat{d}_B^2 = (tr_0)^T$.

3 Discrete conservation laws on n-complexes

We study systems of two conservation laws in integral PH form (4) on an n-dimensional domain $\Omega \subset \mathbb{R}^n$. We consider the cases $p = n \in \{1, 2, 3\}$, $q = 1$ and illustrate the approach at the example $n = 2$ on rectangular grids, before we state the general result.

3.1 Mixed boundary inputs

Constructing the dual n-complexes as sketched above, we can observe the following concerning the inputs for the integral PH formulation of the conservation laws. If *all the n-cells* on the primal complex are integration domains for the conserved quantity α_p, then the boundary inputs will be *exclusively* related to the $(n−1)$-cochain representing the integrals of e_q on the boundary. Correspondingly for α_q on the dual 1-cells and the 0-cochain of boundary values of e_p. This situation of a *unique causality* of the boundary ports is treated in the previous works van der Schaft and Maschke (2011) and Seslija et al. (2014).

However, in most practical cases for modeling and control, a given physical variable will play the role of an input on parts of the boundary, while its power-conjugate will be the input on the rest. The causality along the boundary depends on the boundary conditions which shall be imposed. This situation is designated *mixed inputs* and must be accounted for in the formulation of the dual complexes relative to the system boundary.

---

[11] We denote all quantities on the dual complex (in particular the dual n-cells and the (co)incidence maps) with a "hat".
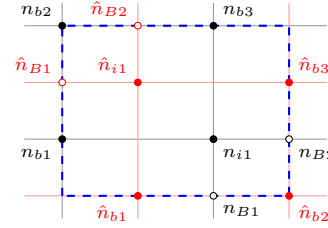
Fig. 3. Definition of nodes on the primal and dual 2-complex

3.2 Construction of the dual complexes

Based on two given staggered meshes and the system boundary, we will construct two n-complexes, the first one representing the integration domains (n-cells) for α_p and their boundary $(n−1)$-cells, associated to e_q. The second (or dual) n-complex contains the integration domains (1-cells) for α_q and their boundaries (0-cells) at which the function values of e_p are evaluated. To define the different subsets of j-cells, related to state and co-state variables, boundary in- and outputs, we exploit topological duality on both complexes and the boundary. The classification of cells on the primal and dual complex, as illustrated below for $n = 2$, can be adapted in a straightforward manner for the other cases $n = 1$ and $n = 3$.

3.2.1 Example: Two-dimensional rectangular grids

We adopt the notation from the previous section with a "hat" for quantities on the dual complex and refer to 0-/1-/2-cells as nodes/edges/faces. Figure 3 shows two staggered rectangular grids (primal: black, dual: red) with their nodes. The system boundary (dashed blue) coincides everywhere with either a line of the primal or the dual mesh. The classification of primal and dual j-cells, as introduced below, is illustrated in Figs. 4 and 5.

Classification of j-cells

We classify the different sets of j-cells as follows. The indices i and b denote *interior* and *boundary* objects that are constructed based on nodes of the primal and dual grid that lie *within* or *on* the system boundary. The capital letter B refers to *additional* (or complementary) boundary nodes and edges.

1. **Nodes.** $n_{i,\cdot} \in \mathcal{N}_i$ and $n_{b,\cdot} \in \mathcal{N}_b$: Nodes of the primal mesh, within and on the boundary.
   $\hat{n}_{i,\cdot} \in \hat{\mathcal{N}}_i$, $\hat{n}_{b,\cdot} \in \hat{\mathcal{N}}_b$: Nodes of the dual mesh, within and on the boundary.

2. **Additional boundary nodes.** $n_{B,\cdot} \in \mathcal{N}_B$ and $\hat{n}_{B,\cdot} \in \hat{\mathcal{N}}_B$: Additional nodes on the intersection of interior edges and the system boundary.
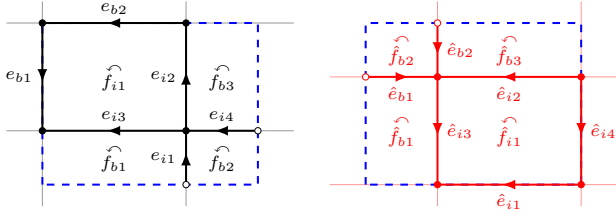
Fig. 4. Interior and boundary edges
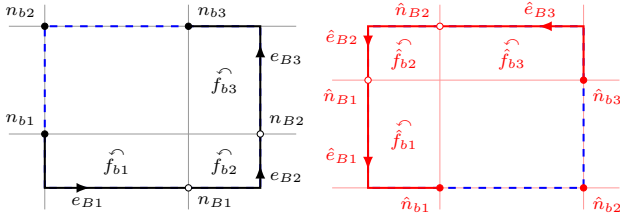
Fig. 5. Complementary boundary edges

3. **Primal edges.** $e_{i,\cdot} \in \mathcal{E}_i$ and $e_{b,\cdot} \in \mathcal{E}_b$, *interior* and *boundary* edges: Connect the above-defined primal nodes and lie *within* and *on* the system boundary, respectively.

4. **Dual edges.** $\hat{e}_{i,\cdot} \in \hat{\mathcal{E}}_i$ and $\hat{e}_{b,\cdot} \in \hat{\mathcal{E}}_b$: Connect the above-defined dual nodes. Their indices follow from topological duality to the primal edges $e_{i,\cdot} \in \mathcal{E}_i$ and $e_{b,\cdot} \in \mathcal{E}_b$.

5. **Faces.** $\hat{f}_{i,\cdot} \in \hat{\mathcal{F}}_i$ and $\hat{f}_{b,\cdot} \in \hat{\mathcal{F}}_b$: Dual faces, topologically dual to primal nodes $n_{i,\cdot} \in \mathcal{N}_i$ and $n_{b,\cdot} \in \mathcal{N}_b$. $f_{i,\cdot} \in \mathcal{F}_i$ and $f_{b,\cdot} \in \mathcal{F}_b$: Primal faces, topologically dual to dual nodes $\hat{n}_{i,\cdot} \in \hat{\mathcal{N}}_i$ and $\hat{n}_{b,\cdot} \in \hat{\mathcal{N}}_b$.

6. **Additional boundary edges.** $e_{B,\cdot} \in \mathcal{E}_B$ and $\hat{e}_{B,\cdot} \in \hat{\mathcal{E}}_B$: Edges (more precisely 1-cells) on the system boundary that complete the boundaries of the faces $f_{b,\cdot} \in \mathcal{F}_b$ and $\hat{f}_{b,\cdot} \in \hat{\mathcal{F}}_b$.

Table 1 shows the cardinalities of the defined sets of j-cells on both complexes, and thereby illustrates the duality between the different cells. By the proposed construction, the following objects are topologically dual *on the boundary*: $\hat{n}_{b,\cdot}$ and $e_{B,\cdot}$ / $\hat{n}_{B,\cdot}$ and $e_{b,\cdot}$ / $n_{b,\cdot}$ and $\hat{e}_{B,\cdot}$ / $n_{B,\cdot}$ and the edges $\hat{e}_{i,\cdot}$ *on the system boundary*.

Incidence matrices

The primal and dual 2-complex in the example have the following incidence matrices (faces to edges and edges to nodes), for which the complex property $\partial_1 \circ \partial_2 = 0$ and $\hat{\partial}_1 \circ \hat{\partial}_2 = 0$ can be immediately verified:

$$
\partial_2 = \left[\begin{array}{cccc}
0 & 1 & -1 & 0 \\
1 & 0 & 0 & -1 \\
-1 & 1 & 0 & 0 \\
0 & 0 & 1 & -1 \\
\hline
1 & 0 & 0 & 0 \\
1 & 0 & 0 & 0 \\
\hline
0 & 1 & 0 & 0 \\
0 & 0 & 1 & 0 \\
0 & 0 & 0 & 1
\end{array}\right],
$$

$$
\partial_1 = \left[\begin{array}{cccc|cc|ccc}
1 & -1 & -1 & 1 & 0 & 0 & 0 & 0 & 0 \\
0 & 0 & 1 & 0 & 1 & 0 & -1 & 0 & 0 \\
0 & 0 & 0 & 0 & -1 & 1 & 0 & 0 & 0 \\
0 & 1 & 0 & 0 & 0 & -1 & 0 & 0 & 1 \\
-1 & 0 & 0 & 0 & 0 & 0 & 1 & -1 & 0 \\
0 & 0 & 0 & -1 & 0 & 0 & 0 & 1 & -1
\end{array}\right],
$$

$$
\hat{\partial}_2 = \left[\begin{array}{c|ccc}
-1 & 0 & 0 & 0 \\
1 & 0 & 0 & -1 \\
1 & -1 & 0 & 0 \\
-1 & 0 & 0 & 0 \\
\hline
0 & -1 & 1 & 0 \\
0 & 0 & -1 & 1 \\
\hline
0 & 1 & 0 & 0 \\
0 & 0 & 1 & 0 \\
0 & 0 & 0 & 1
\end{array}\right],
$$

$$
\hat{\partial}_1 = \left[\begin{array}{cccc|cc|ccc}
0 & 1 & -1 & 0 & 1 & 1 & 0 & 0 & 0 \\
1 & 0 & 1 & 0 & 0 & 0 & 1 & 0 & 0 \\
-1 & 0 & 0 & 1 & 0 & 0 & 0 & 0 & 0 \\
0 & -1 & 0 & -1 & 0 & 0 & 0 & 0 & -1 \\
0 & 0 & 0 & 0 & -1 & 0 & -1 & 1 & 0 \\
0 & 0 & 0 & 0 & 0 & -1 & 0 & -1 & 1
\end{array}\right].
$$

Incidence submatrices

The incidence matrices ∂_j on the primal complex are partitioned according to the involved j- and $(j-1)$-chains,

$$
\partial_2 = \left[\begin{array}{cc}
\partial_2^{ii} & \partial_2^{ib} \\
\partial_2^{bi} & 0 \\
\hline
0 & I
\end{array}\right], \quad
\partial_1 = \left[\begin{array}{cc|c}
\partial_1^{ii} & 0 & 0 \\
\partial_1^{bi} & \partial_1^{bb} & \partial_1^{bB} \\
\partial_1^{Bi} & 0 & \partial_1^{BB}
\end{array}\right]. \quad (17)
$$

The zero matrices and the identity matrix result from the construction of the subsets[12] indexed i, b and B. On the dual complex, the structure of the incidence matrices is

$$
\hat{\partial}_2 = \left[\begin{array}{cc}
\hat{\partial}_2^{ii} & \hat{\partial}_2^{ib} \\
0 & \hat{\partial}_2^{bb} \\
\hline
0 & I
\end{array}\right], \quad
\hat{\partial}_1 = \left[\begin{array}{cc|c}
\hat{\partial}_1^{ii} & \hat{\partial}_1^{ib} & 0 \\
\hat{\partial}_1^{bi} & 0 & \hat{\partial}_1^{bB} \\
\hline
0 & -I & \hat{\partial}_1^{BB}
\end{array}\right]. \quad (18)
$$

---

12 $\partial_2^{bb} = 0$ as the b-edges lie on the boundary of i-faces. $\partial_2^{Bi} = 0$ as the B-edges lie on the boundary of the b-faces. $\partial_2^{Bb} = I$ by definition of the B-edges to complete the boundary of the positively oriented b-faces. $\partial_1^{ib} = 0$ and $\partial_1^{iB} = 0$ as i-nodes are at the terminals of i-edges only. $\partial_1^{Bb} = 0$ as the b-edges are terminated only by b-nodes.

Table 1. Cardinalities of the sets of primal and dual j-cells

Primal	$\mathcal{N}_i$	$\mathcal{N}_b$	$\mathcal{N}_B$	$\mathcal{F}_i$	$\mathcal{F}_b, \mathcal{E}_B$		$\mathcal{E}_i$	$\mathcal{E}_b$
Dual	$\hat{\mathcal{F}}_i$	$\hat{\mathcal{F}}_b, \hat{\mathcal{E}}_B$		$\hat{\mathcal{N}}_i$	$\hat{\mathcal{N}}_b$	$\hat{\mathcal{N}}_B$	$\hat{\mathcal{E}}_i$	$\hat{\mathcal{E}}_b$
#	1	3	2	1	3	2	4	2

The different locations of the zero matrices result from the definition of dual objects. For example b-indexed edges on the dual complex do not lie on its boundary. $\hat{\partial}_1^{Bb} = -I$ comes from the one-to-one relation of B-nodes and b-edges on the dual complex, and the orientation of the edges $\hat{e}_{b,\cdot}$, which is induced by the positive orientation of the primal boundary.

3.2.2 Duality relations of incidence submatrices

Using the duality relations (15), (16), and based on an analogous construction of the dual complexes for $n \in \{1, 2, 3\}$, the following duality relations between the (co-) incidence submatrices can be given. Given the incidence matrices (on either the primal or the dual complex), the co-incidence matrices result from transposition:

$$\mathrm{d}_{\alpha\beta}^j = (\partial_j^{\beta\alpha})^T, \qquad \alpha, \beta \in \{i, b, B\}. \tag{19}$$

The submatrices of ∂_j and d^j (upper or upper left submatrices in the above example) that relate i and b indexed cells will be designated (i, b). As the relations between the i and b indexed cells are well-defined by topological duality, Eq. (15) applies accordingly:

$$\hat{\mathrm{d}}_{(i,b)}^j = (-1)^{n-j+1} (\mathrm{d}_{(i,b)}^{n-j+1})^T. \tag{20}$$

For the dual co-incidence matrices that relate b-indexed $(j-1)$-cells (in the interior) and B-indexed j-cells (on the boundary), the following holds:

$$\hat{\mathrm{d}}_{bB}^j = (-1)^{n-j} I. \tag{21}$$

This relation corresponds to Eq. (16), where the trace matrix boils down to the identity matrix due to the fact that *all* B-indexed cells live on the boundary.

3.3 Discrete PH representation

The integral conservation laws are now written in a compact form, exploiting the topological description of the primal and dual mesh in terms of dual n-complexes. We introduce the following notation. $\boldsymbol{P}_i \in \mathbb{R}^{|\mathcal{F}_i|}$, $\boldsymbol{P}_b \in \mathbb{R}^{|\mathcal{F}_b|}$ and $\hat{\boldsymbol{Q}}_i \in \mathbb{R}^{|\hat{\mathcal{E}}_i|}$, $\hat{\boldsymbol{Q}}_b \in \mathbb{R}^{|\hat{\mathcal{E}}_b|}$ are vector representations of the primal 2-cochains and dual 1-cochains that correspond to the integral conserved quantities on the primal 2-cells and dual 1-cells. $\boldsymbol{e}_i^q \in \mathbb{R}^{|\mathcal{E}_i|}$, $\boldsymbol{e}_b^q \in \mathbb{R}^{|\mathcal{E}_b|}$, $\boldsymbol{e}_B^q \in \mathbb{R}^{|\mathcal{E}_B|}$ and $\hat{\boldsymbol{e}}_i^p \in \mathbb{R}^{|\hat{\mathcal{N}}_i|}$, $\hat{\boldsymbol{e}}_b^p \in \mathbb{R}^{|\hat{\mathcal{N}}_b|}$, $\hat{\boldsymbol{e}}_B^p \in \mathbb{R}^{|\hat{\mathcal{N}}_B|}$ are the vector representations of the primal 1-cochains and dual 0-cochains with the values of the boundary fluxes to the

integration domains (the co-energy variables at the integration boundaries). For the "interior" integration domains we obtain, combining the integral representation (4), the definition of flux functions (6), and the topology in terms of the co-incidence matrices,

$$\dot{\boldsymbol{P}}_i = \mathrm{d}_{ii}^p(-1)^{pq}\boldsymbol{e}_i^q + \mathrm{d}_{ib}^p(-1)^{pq}\boldsymbol{e}_b^q \tag{22a}$$

$$\dot{\boldsymbol{Q}}_i = -\hat{\mathrm{d}}_{ii}^q\hat{e}_i^p - \hat{\mathrm{d}}_{ib}^q\hat{e}_b^p. \tag{22b}$$

Accordingly for the "boundary" integration domains:

$$\dot{\boldsymbol{P}}_b = \mathrm{d}_{bi}^p(-1)^{pq}\boldsymbol{e}_i^q + \mathrm{d}_{bB}^p(-1)^{pq}\boldsymbol{e}_B^q \tag{23a}$$

$$\dot{\boldsymbol{Q}}_b = -\hat{\mathrm{d}}_{bi}^q\hat{e}_i^p - \hat{\mathrm{d}}_{bB}^q\hat{e}_B^p. \tag{23b}$$

Applying the duality relations

$$\hat{\mathrm{d}}_{ii}^q = (-1)^p(\mathrm{d}_{ii}^p)^T,$$
$$\hat{\mathrm{d}}_{ib}^q = (-1)^p(\mathrm{d}_{bi}^p)^T, \quad \hat{\mathrm{d}}_{bi}^q = (-1)^p(\mathrm{d}_{ib}^p)^T, \tag{24}$$

as well as

$$\mathrm{d}_{bB}^p = \boldsymbol{I}, \quad \hat{\mathrm{d}}_{bB}^q = (-1)^{p-q}\boldsymbol{I}, \tag{25}$$

we can write

$$\frac{d}{dt}\begin{bmatrix}\boldsymbol{P}_i \\ \hat{\boldsymbol{Q}}_i\end{bmatrix} = \begin{bmatrix}0 & \mathrm{d}_{ii}^p \\ -(\mathrm{d}_{ii}^p)^T & 0\end{bmatrix}\begin{bmatrix}(-1)^p\hat{e}_i^p \\ (-1)^{pq}\boldsymbol{e}_i^q\end{bmatrix}$$
$$+ \begin{bmatrix}0 & \mathrm{d}_{ib}^p \\ -(\mathrm{d}_{bi}^p)^T & 0\end{bmatrix}\begin{bmatrix}(-1)^p\hat{e}_b^p \\ (-1)^{pq}\boldsymbol{e}_b^q\end{bmatrix} \tag{26a}$$

and

$$\begin{bmatrix}(-1)^{pq}\boldsymbol{e}_B^q - \frac{d}{dt}\boldsymbol{P}_b \\ -(-1)^{p-q}\hat{e}_B^p - \frac{d}{dt}\hat{\boldsymbol{Q}}_b\end{bmatrix} = \begin{bmatrix}0 & -\mathrm{d}_{bi}^p \\ (\mathrm{d}_{ib}^p)^T & 0\end{bmatrix}\begin{bmatrix}(-1)^p\hat{e}_i^p \\ (-1)^{pq}\boldsymbol{e}_i^q\end{bmatrix}. \tag{26b}$$

We can now state the following main result:

Proposition 1. *The discrete formulation of a system of two conservation laws with $p = n \in \{1, 2, 3\}$, $q = 1$ on two staggered grids with a system boundary that gives rise to the definition of a primal and a dual n-complex as sketched above, reads*

$$\underbrace{\frac{d}{dt}\begin{bmatrix}\boldsymbol{P}_i \\ \hat{\boldsymbol{Q}}_i\end{bmatrix}}_{\dot{x}} = (-1)^n \underbrace{\begin{bmatrix}0 & \mathrm{d}_{ii}^n \\ -(\mathrm{d}_{ii}^n)^T & 0\end{bmatrix}}_{J}\underbrace{\begin{bmatrix}\hat{e}_i^p \\ \boldsymbol{e}_i^q\end{bmatrix}}_{e}$$
$$+ (-1)^n \underbrace{\begin{bmatrix}0 & \mathrm{d}_{ib}^n \\ -(\mathrm{d}_{bi}^n)^T & 0\end{bmatrix}}_{G}\underbrace{\begin{bmatrix}\hat{e}_b^p \\ \boldsymbol{e}_b^q\end{bmatrix}}_{u} \tag{27a}$$

$$\underbrace{(-1)^n\begin{bmatrix}\boldsymbol{e}_B^q \\ \hat{e}_B^p\end{bmatrix} - \frac{d}{dt}\begin{bmatrix}\boldsymbol{P}_b \\ \hat{\boldsymbol{Q}}_b\end{bmatrix}}_{y} = (-1)^n \underbrace{\begin{bmatrix}0 & -\mathrm{d}_{bi}^n \\ (\mathrm{d}_{ib}^n)^T & 0\end{bmatrix}}_{G^T}\underbrace{\begin{bmatrix}\hat{e}_i^p \\ \boldsymbol{e}_i^q\end{bmatrix}}_{e}. \tag{27b}$$

$\boldsymbol{d}_{ii}^n, \boldsymbol{d}_{ib}^n, \boldsymbol{d}_{bi}^n$ *are co-incidence matrices relating $(n-1)$-cells and n-cells on the primal complex.* $\boldsymbol{P}_{i/b}$, $\hat{\boldsymbol{Q}}_{i/b}$, $\boldsymbol{e}_{i/b/B}^q$,

$\hat{e}^p_{i/b/B}$, *are vector representations of the j-cochains with the integral values of the n-forms, 1-forms, $(n-1)$-forms and 0-forms on the corresponding discrete objects (j-chains) of the primal and dual complex.*

Proof. Primal and dual n-complex can be constructed in analogy to above for $n = 1$ and $n = 3$ with complete duality between i and b indexed cells and the definition of B indexed cells. This allows to apply the duality formulas (20), (21) to (26a), (26b), which yields (27a), (27b). □

The discrete formulation of the system of two conservation laws is *exact*. It is written in form of the input-output representation of a finite-dimensional Dirac structure for which the power balance $-e^T \dot{x} + y^T u = 0$ holds. However, it can not be understood as a finite-dimensional PH system, as the vector of co-energy variables e is *not* derived from a finite-dimensional energy function. A finite-dimensional PH system is obtained if the energy functional is replaced by a finite-dimensional approximation and discrete constitutive relation are established. In other words, or more general, the true boundary fluxes at the integration domains have to be replaced by numerical flux functions, which is the key ingredient of classical finite volume discretization.

Remark 5. The *collocated* pairs of boundary variables $(\hat{e}^p_b, e^q_B)$ and $(e^q_b, \hat{e}^p_B)$ are *not exactly power-conjugated*. This is due to the presence of $\frac{d}{dt}P_b$ and $\frac{d}{dt}\hat{Q}_b$ in the output equation[13]. Vice-versa, y does not exactly represent fluxes at the system boundary. This effect, which is due to the staggered dual grids, decreases with grid refinement.

Remark 6. The results from Seslija et al. (2014) with identical boundary inputs can be recovered if the system boundary is drawn exclusively along $(n-1)$-cells of the primal *or* the dual mesh.

4 Numerical approximation

The topological information, coded in the primal and dual n-complex yields the *exact* discrete formulation of the two conservation laws in input-/output form (27a), (27b). The elements of the state vector x and the co-state/effort vector e are the *integral quantities* on the integration domains of the primal and dual mesh. However, the constitutive relations (5) are formulated *locally* between the corresponding differential forms.

For a *numerical approximation* model in PH form, a *discrete energy* must be defined in terms of the discrete states, and the discrete efforts must be derived from this approximate energy. We present this *structure-preserving* discretization of the constitutive equations on the example of the 2D shallow water equations, and discuss its properties, in particular the relation of some aspects to "classical" finite volume schemes.

Remark 7. In Seslija et al. (2014), a *quadratic* discrete energy is directly expressed in terms of the cochains on both complexes. The *linear* constitutive relations are expressed involving the *discrete Hodge operator*[14]. Such a *direct formulation* of the approximate energy is less obvious for non-quadratic energies and spatial dependencies.

4.1 Example: 2D shallow water equations

Consider the 2D shallow water equations (SWE) in standard vector calculus form[15]

$$\begin{bmatrix} \partial_t s \\ \partial_t u + q F^{\perp} \end{bmatrix} = \begin{bmatrix} 0 & -\mathrm{div} \\ -\mathrm{grad} & 0 \end{bmatrix} \begin{bmatrix} \frac{1}{2}u \cdot u + gs + gb \\ su \end{bmatrix}, \quad (28)$$

where $s(x, y)$ denotes the elevation of the free water surface over the bottom profile $b(x, y)$, $u(x, y) = [u(x, y) \quad v(x, y)]^T$ is the 2-dimensional velocity vector and g the gravitational acceleration. The term $qF^{\perp}$ with $F^{\perp} = [sv \quad -su]^T$ represents the acceleration due to rotation of the flow and stems from the transport term in the momentum equation. $q = \frac{1}{s}(\partial_x v - \partial_y u)$ denotes the *potential vorticity*[16]. The vector on the right of (28) contains the hydrodynamic pressure p_{dyn} and the vector of discharge per unit width in x- and y- direction. p_{dyn} and the components of su can be expressed as variational derivatives of the Hamiltonian H (equivalently partial derivatives of the Hamiltonian density $\mathcal{H}$) with respect to s, u and v with the energy per unit mass

$$H = \int_{\Omega} \mathcal{H} \, dx dy, \qquad \mathcal{H} = \frac{1}{2}su^2 + \frac{1}{2}gs^2 + gsb. \quad (29)$$

We consider a rectangular domain $\Omega \subset \mathbb{R}^2$. For flow problems with negligible rotational acceleration $qF^{\perp}$, the SWE have the canonical form of a PH system (8a) with $n = p = 2$, $q = 1$. The states and co-states in terms of

---

13 In Seslija et al. (2014), this fact is less obvious.

14 See Desbrun et al. (2005), Definition 6.1.

15 See e. g. Arakawa and Lamb (1981).

16 It satisfies the balance equation $\partial_t q + u \cdot \nabla q = 0$, i. e. it is advected with the fluid flow see e. g. Arakawa and Lamb (1981). It plays an important role in the long-time numerical simulation of large scale flow problems.
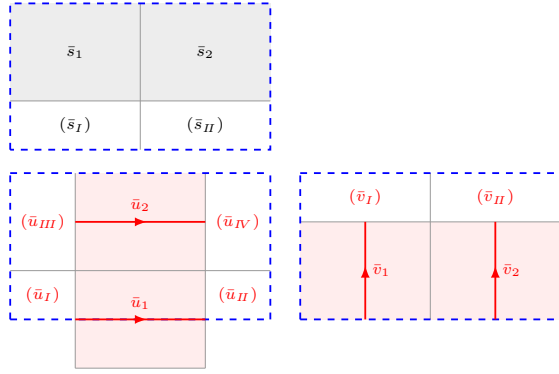
Fig. 6. 2D (sub-)domains associated with the discrete states

Fig. 7. 2D control volumes with multi-index $I = (j, k, l)$. A point $\cdot$ denotes that the corresponding state is not needed to compute an effort. Black and red: Discrete efforts computed from $\nabla H(\boldsymbol{x}_d)$. As it does not affect a state differential equation, $e_{d,1}^u$ is set in parentheses. Blue: Boundary efforts = input variables.

differential forms[17] are then $\alpha_p = *s$, $\alpha_q = \boldsymbol{u}^\flat$, $e_p = p_{dyn}$ and $e_q = -(*(s\boldsymbol{u})^\flat)$. For brevity, we assume $b(x, y) \equiv 0$.

4.2 Finite-dimensional PH model

We consider uniform rectangular grids that are shifted by half the grid size $\Delta x/2$ and $\Delta y/2$ in each direction. The discrete state vector $\boldsymbol{x}_d = \begin{bmatrix} \boldsymbol{S}_d^T & \boldsymbol{U}_d^T & \boldsymbol{V}_d^T \end{bmatrix}^T$ with components $S_{d,j}$, $j = 1, \ldots, |\mathcal{F}_i|$, $U_{d,k}$, $k = 1, \ldots, |\hat{\mathcal{E}}_i^x|$, and $V_{d,l}$, $l = 1, \ldots, |\hat{\mathcal{E}}_i^y|$, represents the approximate area integrals of s on the interior primal faces and the approximate line integrals of u and v on the horizontal/vertical interior edges of the dual grid. Denote $\bar{\boldsymbol{x}} = \begin{bmatrix} \bar{\boldsymbol{s}}^T & \bar{\boldsymbol{u}}^T & \bar{\boldsymbol{v}}^T \end{bmatrix}^T$ the vector of *average* states on the corresponding primal 2-cells and dual 1-cells, which are given by

$$\bar{s}_j = \frac{S_{d,j}}{\Delta x \Delta y}, \quad \bar{u}_k = \frac{U_{d,k}}{\Delta x}, \quad \bar{v}_l = \frac{V_{d,l}}{\Delta y}, \qquad (30)$$

where $\Delta x \Delta y = |f_j|$ is the area of a primal face and $\Delta x = |\hat{e}_k^x|$, $\Delta y = |\hat{e}_l^y|$ are the lengths of the dual edges. We understand the average state values as approximations of $s(x, y)$, $u(x, y)$ and $v(x, y)$ on the interior primal faces and the surrounding areas of the dual interior edges, respectively. These domains may lie partially outside Ω, see the shaded regions in Fig. 6. The superposition of the dual grids divides the whole spatial domain into *control volumes* with identical values of average states, indexed $I = (j, k, l) \in \mathcal{I}$, see the Fig. 7. Their sizes for regular, uniformly shifted grids is $\Delta x \Delta y / 4$.

We define the *discrete Hamiltonian* as

$$H_d(\boldsymbol{x}_d) = \frac{\Delta x \Delta y}{4} \sum_{I \in \mathcal{I}} \mathcal{H}\left(\frac{S_{d,j(I)}}{\Delta x \Delta y}, \frac{U_{d,k(I)}}{\Delta x}, \frac{V_{d,l(I)}}{\Delta y} \right), \quad (31)$$

where $j(I)$, $k(I)$, $l(I)$ are the components of the multi-index I. In the boundary regions, where no discrete states are defined, we need to impose additional *ghost values* for the states, denoted in brackets in Fig. 6. We assign *constant* ghost values, based on reasonable assumptions, e.g. given boundary conditions or the steady state. The consistency of the effort approximation depends on the validity of these assumptions, see further below.

Remark 8. Usually, the ghost values are computed by extrapolation from the interior discrete states[18]. We could do accordingly, and assign the adjacent discrete states to the ghost cells (zero order extrapolation). For a consistent energy approximation, this would impose an enlargement of the j-cells to which the discrete states are associated. This re-interpretation of the discrete states and their spatial domains is, however, not consistent with the exact PH representation of the conservation laws (27a), (27b).

The vector of *discrete efforts* is derived from the discrete Hamiltonian, $\begin{bmatrix} (\boldsymbol{e}_d^s)^T & (\boldsymbol{e}_d^u)^T & (\boldsymbol{e}_d^v)^T \end{bmatrix}^T = \boldsymbol{e}_d := \nabla H_d(\boldsymbol{x}_d)$. In particular, we express the single discrete efforts as

$$e_{d,j}^s := \frac{\partial H_d}{\partial S_{d,j}} = \sum_{I \in \mathcal{I}_j^s} \frac{\Delta x \Delta y}{4} \frac{1}{\Delta x \Delta y} \left. \frac{\partial \mathcal{H}}{\partial s} \right|_{\bar{\boldsymbol{x}}_I},$$

$$e_{d,k}^u := \frac{\partial H_d}{\partial U_{d,k}} = \sum_{I \in \mathcal{I}_k^u} \frac{\Delta x \Delta y}{4} \frac{1}{\Delta x} \left. \frac{\partial \mathcal{H}}{\partial u} \right|_{\bar{\boldsymbol{x}}_I},$$

$$e_{d,l}^v := \frac{\partial H_d}{\partial V_{d,l}} = \sum_{I \in \mathcal{I}_l^v} \frac{\Delta x \Delta y}{4} \frac{1}{\Delta y} \left. \frac{\partial \mathcal{H}}{\partial v} \right|_{\bar{\boldsymbol{x}}_I}. \qquad (32)$$

The notation $(\cdot)|_{\bar{\boldsymbol{x}}_I}$ denotes the evaluation of the partial derivatives of $\mathcal{H}$ at $(\bar{s}_j, \bar{u}_k, \bar{v}_l) = \left(\frac{S_{d,j(I)}}{\Delta x \Delta y}, \frac{U_{d,k(I)}}{\Delta x}, \frac{V_{d,l(I)}}{\Delta y} \right)$.

---

17 The Hodge star $*$ converts a k-form to a $(n-k)$-form, index lowering $\flat$ generates the 1-form associated to a vector field, vice-versa index raising $\sharp$. With these operations, the vector calculus operators div and grad can be expressed in terms of the exterior derivative d. For details see e.g. Holm (2011).

18 See e.g. LeVeque (2002), Chapter 7.

$\mathcal{I}_j^s$, $\mathcal{I}_k^u$ and $\mathcal{I}_l^v$ are the sets of multi-indices that refer to the 2×2 control volumes associated with $S_{d,j}$, $U_{d,k}$ or $V_{d,l}$, respectively. For the corresponding average efforts $\bar{e} = \left[(e_d^s)^T \quad \frac{(e_d^u)^T}{\Delta y} \quad \frac{(e_d^v)^T}{\Delta x} \right]^T$, we obtain

$$\bar{e}_j^s = \sum_{I \in \mathcal{I}_j^s} \frac{1}{4} \left. \frac{\partial \mathcal{H}}{\partial s} \right|_{\bar{\boldsymbol{x}}_I}, \quad \bar{e}_k^u = \sum_{I \in \mathcal{I}_k^u} \frac{1}{4} \left. \frac{\partial \mathcal{H}}{\partial u} \right|_{\bar{\boldsymbol{x}}_I}, \quad \bar{e}_l^v = \sum_{I \in \mathcal{I}_l^v} \frac{1}{4} \left. \frac{\partial \mathcal{H}}{\partial v} \right|_{\bar{\boldsymbol{x}}_I}. \tag{33}$$

Proposition 2. *The finite-dimensional PH model*

$$\dot{\boldsymbol{x}}_d = \boldsymbol{J} \boldsymbol{e}_d + \boldsymbol{G} \boldsymbol{u}_d \tag{34a}$$

$$\boldsymbol{y}_d = \boldsymbol{G}^T \boldsymbol{e}_d, \tag{34b}$$

with $\boldsymbol{J}$ *and* $\boldsymbol{G}$ *as defined in* (27a), (27b), *and* $\boldsymbol{e}_d = \nabla H_d(\boldsymbol{x})$ *derived from the discrete Hamiltonian* (31), *is a consistent approximation of the 2D SWE, if the ghost values on the boundary control volumes are chosen consistent with the boundary conditions.*

Proof. We sketch the proof of this statement on consistency order. To this end, we consider the differential equation of the finite-dimensional PH model in terms of the *average* states and efforts (see Appendix A.1):

$$\dot{\bar{\boldsymbol{x}}} = \frac{1}{\Delta x} \bar{\boldsymbol{J}} \bar{\boldsymbol{e}} + \frac{1}{\Delta x} \bar{\boldsymbol{G}} \bar{\boldsymbol{u}}, \tag{35}$$

where the elements of $\bar{\boldsymbol{J}}$, $\bar{\boldsymbol{G}}$ are in $\{0, \pm 1, \pm \frac{\Delta y}{\Delta x}\}$. The (local) approximation error, which determines the consistency order[19] is

$$\epsilon_{loc} = \| \dot{\bar{\boldsymbol{x}}}^* - \frac{1}{\Delta x} \bar{\boldsymbol{J}} \, \bar{\boldsymbol{e}}|_* - \frac{1}{\Delta x} \bar{\boldsymbol{G}} \, \bar{\boldsymbol{u}}|_* \|_{\Delta x} \tag{36}$$

for $\Delta x \to 0$. $\dot{\bar{\boldsymbol{x}}}^*$ contains the time derivatives of the *exact solution* at the centers of the 2×2 control volumes, and is given by the right hand side of the PDE (28). The average efforts $\bar{\boldsymbol{e}}$ are computed based on the true solution of the PDE. The $*$ denotes the replacement

$$* = \Big(\bar{s}_j = \int_{y_{j,low}^s}^{y_{j,up}^s} \int_{x_{j,lef}^s}^{x_{j,rig}^s} \frac{s(x,y)}{\Delta x \Delta y} \, dx dy,$$

$$\bar{u}_k = \int_{x_{k,lef}^u}^{x_{k,rig}^u} \frac{u(x, y_k^u)}{\Delta x} \, dx, \quad \bar{v}_l = \int_{y_{l,low}^v}^{y_{l,up}^v} \frac{v(x_l^v, y)}{\Delta y} \, dy \Big). \tag{37}$$

The limits of integration with the subscripts lef, rig, low, up refer to the boundaries of the considered 2×2 control volume in x- and y-direction. y_k^u and x_l^v denote the corresponding center coordinates. The norm

$$\|\boldsymbol{f}\|_{\Delta x} := \left(\Delta x \sum_{j=1}^N |f_j| \right)^{\frac{1}{2}} \tag{38}$$

is the discrete counterpart of the L^2-norm for functions. Assuming the boundary inputs exactly known, they cancel from (36). The order of the error ϵ_{loc} is certainly $\mathcal{O}(\Delta x^p)$, if for all *integer* j, k, l, the errors

$$\epsilon_j^{s,x} = \left| \frac{\partial}{\partial x} e_j^s - \frac{1}{\Delta x} \left. \bar{e}_j^s \right|_* \right|_{\Delta x}, \quad \epsilon_j^{s,y} = \left| \frac{\partial}{\partial y} e_j^s - \frac{1}{\Delta y} \left. \bar{e}_j^s \right|_* \right|_{\Delta x}$$

$$\epsilon_k^u = \left| \frac{\partial}{\partial x} e_k^u - \frac{1}{\Delta x} \left. \bar{e}_k^u \right|_* \right|_{\Delta x},$$

$$\epsilon_v^l = \left| \frac{\partial}{\partial y} e_l^v - \frac{1}{\Delta y} \left. \bar{e}_l^v \right|_* \right|_{\Delta x} \tag{39}$$

are of order $\mathcal{O}(\Delta x^p)$ for $\Delta x, \Delta y \to 0$. We denote e_j^s, e_k^u, e_l^v the *true* efforts at the centers of the 2×2 control volumes. By Taylor series expansion, it can be verified that on superposed, regular grid with constant grid size $\frac{\Delta x}{2} \times \frac{\Delta y}{2}$, the errors (39) are of order $\mathcal{O}(\Delta x^2)$, if their computation does *not* involve ghost values for the average states. If the shifts between primal and dual grid are different from $\frac{\Delta x}{2}, \frac{\Delta y}{2}$, the order decreases to $\mathcal{O}(\Delta x)$. If the discrete efforts are computed based on ghost values, the consistency error is of order ≥ 1 only if the ghost values are consistent with the boundary conditions. In Appendix A.2, the computations of three consistency errors for the efforts depicted in Fig. 7 are sketched: based on (i) no, (ii) consistent, and (iii) inconsistent ghost values.   □

4.3 Remarks

The numerical approximation of the Hamiltonian and the efforts, and the subsequent consistency analysis, give rise to the following complementary remarks.

1. The output equation of the discretized average model is simply written $\bar{\boldsymbol{y}} = \boldsymbol{G}^T \bar{\boldsymbol{e}}$, without scaling. Assigning constant ghost values for the states on the boundary integration domains corresponds to $\frac{d}{dt} \boldsymbol{P}_b = \boldsymbol{0}$, $\frac{d}{dt} \hat{\boldsymbol{Q}}_b = \boldsymbol{0}$ in (27b). Consequently, $\boldsymbol{y}_d$ and $\bar{\boldsymbol{y}}$ can be understood as integral/average numerical approximations of the output boundary efforts for $\Delta x, \Delta y \to 0$.

2. The resulting finite-dimensional model is in PH form, i.e. the discretization scheme is *structure preserving*. The PH structure implies, for H_d positive definite, Lyapunov stability of the unforced equilibrium.

3. For the average discretized model in PH form, *numerical stability* (more precisely, numerical stability of the semi-discretization method, see Iserles (2009), Section 13.2) can be shown: For bounded $\bar{\boldsymbol{u}}(t)$, there exists on every time interval $[0, t^*]$ a bound $c(t^*) < \infty$ such that $\|\bar{\boldsymbol{x}}(t)\|_{\Delta x} < c(t^*)$.

---

19 See Iserles (2009), Eq. (3.19)

4. As discussed above, the consistency order of the effort approximation for the nonlinear SWE is 2 inside the spatial domain. This is due to the uniform shift of the primal and dual grid, which implies a centered approximation of the constitutive equations. The order can be increased by computing the numerical fluxes based on a wider stencil, using a semi-discrete *generalized Leapfrog* scheme, see Iserles (1986), or Fornberg (1990) from the finite-difference perspective and Kotyczka (2016) for the application to 1D PH systems.

5. The grid shifts in x- and y-direction can be understood as design degrees of freedom to parametrize numerical schemes which take into account the direction of propagation (of the solution), in the sense of *upwinding*[20]. For such non-centered schemes, the consistency order inside the spatial domain reduces to 1.

6. The bottleneck for the consistency order of the overall numerical scheme is the assignment of *constant* ghost values, which can be inconsistent with the boundary conditions. The usual approach to extrapolate the ghost values from the interior discrete states, ensures consistency. This measure, however, disturbs the PH structure of the approximate model, as not all numerical fluxes are derived exclusively from the discrete, time-invariant Hamiltonian. The corresponding numerical error acts as a disturbance to the PH model. Its effect can be dissipated if the model contains physical damping/friction.

7. If, as in the acoustic example of Trenchant et al. (2015), the Hamiltonian is separable, the computation of the discrete efforts does not rely on the ghost values, which guarantees consistency of the scheme.

8. For linear PDEs, consistency and numerical stability of the approximation directly imply convergence of the numerical scheme according to the *Lax-Richtmyer equivalence theorem*[21]. For a further discussion on convergence, we refer to the corresponding literature, e. g. Quarteroni and Valli (1994), Eymard et al. (2000), LeVeque (2002), or more specifically, Eymard and Herbin (2005)[22].

5 Conclusions

We proposed the integral/discrete PH formulation of systems of two conservation laws on staggered grids on n-dimensional spatial domains, by using the topological information in terms of (co-)incidence matrices of the related n-complexes. We extended known results by allowing for boundary input variables of mixed type as a basis to tackle a wider class of control problems. We related the numerical approximation of the energy to classical finite volume approaches and determined the consistency order for a nonlinear example in 2D.

The main directions of future work on the numerical side are structured PH modeling and energy approximation on non-regular grids, understanding the shifts between primal and dual grid as design parameters and the relation to other discretization approaches like mixed FEM. For control, issues like structural system properties are of major interest, as well as control design based on the integral formulation of conservation laws.

A Consistency analysis

A.1 Model in terms of average states

We sketch the the transition from the integral to the average model. The matrices $\boldsymbol{J}$ and $\boldsymbol{G}$ in (27a), (34a) for the 2D SWE are partitioned as follows:

$$\boldsymbol{J} = \begin{bmatrix} \boldsymbol{0} & \boldsymbol{J}_1 & \boldsymbol{J}_2 \\ -\boldsymbol{J}_1^T & \boldsymbol{0} & \boldsymbol{0} \\ -\boldsymbol{J}_2^T & \boldsymbol{0} & \boldsymbol{0} \end{bmatrix}, \quad \boldsymbol{G} = \begin{bmatrix} \boldsymbol{0} & \boldsymbol{G}_1 & \boldsymbol{G}_2 \\ \boldsymbol{G}_3 & \boldsymbol{0} & \boldsymbol{0} \\ \boldsymbol{G}_4 & \boldsymbol{0} & \boldsymbol{0} \end{bmatrix}. \quad (40)$$

Integral and average states and efforts are related via

$$\boldsymbol{x}_d = \boldsymbol{\Delta}^x(\Delta x, \Delta y)\bar{\boldsymbol{x}}, \quad \boldsymbol{e}_d = \boldsymbol{\Delta}^e(\Delta x, \Delta y)\bar{\boldsymbol{e}}, \quad (41)$$

where $\boldsymbol{\Delta}^x(\Delta x, \Delta y) := \text{blockdiag}\{\Delta x\Delta y\boldsymbol{I}, \Delta x\boldsymbol{I}, \Delta y\boldsymbol{I}\}$ and $\boldsymbol{\Delta}^e(\Delta x, \Delta y) := \text{blockdiag}\{\boldsymbol{I}, \Delta y\boldsymbol{I}, \Delta x\boldsymbol{I}\}$. Note that $\boldsymbol{\Delta}^x\boldsymbol{\Delta}^e = \Delta x\Delta y\boldsymbol{I}$. With the discrete Hamiltonian density

$$\bar{H}_d(\bar{\boldsymbol{x}}) := \frac{1}{\Delta x\Delta y}H_d(\boldsymbol{\Delta}^x(\Delta x, \Delta y)\bar{\boldsymbol{x}}) \quad (42)$$

such that

$$\nabla\bar{H}_d(\bar{\boldsymbol{x}}) = \frac{1}{\Delta x\Delta y}\boldsymbol{\Delta}^x(\Delta x, \Delta y)\nabla H_d(\boldsymbol{x}_d)$$
$$= (\boldsymbol{\Delta}^e(\Delta x, \Delta y))^{-1}\nabla H_d(\boldsymbol{x}_d), \quad (43)$$

Eq. (34a) transforms to the average model (35) with $\bar{\boldsymbol{e}} := \nabla\bar{H}_d(\bar{\boldsymbol{x}})$ and $\bar{\boldsymbol{J}} = \Delta x(\boldsymbol{\Delta}^x)^{-1}\boldsymbol{J}\boldsymbol{\Delta}^e, \bar{\boldsymbol{G}} = \Delta x(\boldsymbol{\Delta}^x)^{-1}\boldsymbol{G}\boldsymbol{\Delta}^e$. In particular, $\boldsymbol{J} = \bar{\boldsymbol{J}}$ and $\boldsymbol{G} = \bar{\boldsymbol{G}}$ for $\Delta x = \Delta y$.

---

20 We write *in the sense of*, as the grid shift is fixed and based on *a priori* assumptions on the flow direction. For upwinding methods, see e. g. LeVeque (2002), Chapter 4.

21 See Iserles (2009), Section 13.2 for semi-discretization.

22 As a related steady-state problem, the convergence of a centered scheme on two staggered finite volume grids for the incompressible Navier-Stokes equations in 2D is discussed.

A.2 Computations of consistency errors

For the Hamiltonian density (29) with $b \equiv 0$, the average discrete efforts $\bar{e}$ according to (33), have the components

$$
\bar{e}_j^s = \frac{1}{2} \left(\frac{U_{lef}^2 + U_{rig}^2}{2\Delta x^2} + \frac{V_{low}^2 + V_{up}^2}{2\Delta y^2} \right) + \frac{g S_{d,j}}{\Delta x \Delta y}
$$

$$
\bar{e}_k^u = \frac{S_{lef} + S_{rig}}{2\Delta x \Delta y} \frac{U_{d,k}}{\Delta x}
$$

$$
\bar{e}_l^v = \frac{S_{low} + S_{up}}{2\Delta x \Delta y} \frac{V_{d,l}}{\Delta y}. \tag{44}
$$

where lef, rig, low, up refer to the left, right, lower and upper parts of the considered 2×2 control volume. We show the consistency errors for three representative cases of the sample grid shown in Fig. 7. For simplicity, in all three cases, we consider $(x, y) = (0, 0)$ as the center co-ordinates of the 2×2 control volume and we omit the arguments of the functions where clear from the context.

No ghost value

The numerical approximation of the discharge $e_2^u = su$ between the faces f_1 and f_2 on the primal grid does not depend on ghost values. We replace $S_{lef} + S_{rig} = \int_{-\frac{\Delta y}{2}}^{\frac{\Delta y}{2}} \int_{-\Delta x}^{\Delta x} s(x, y)\, dxdy$ and $U_{d,2} = \int_{-\frac{\Delta x}{2}}^{\frac{\Delta x}{2}} u(x, 0)\, dx$ in $\bar{e}_2^u\big|_*$. The Taylor series expansion of

$$
\epsilon_2^u = \left| \frac{\partial e_2^u}{\partial x} \Big|_{(0,0)} - \frac{1}{\Delta x} \bar{e}_2^u \big|_* \right|_{\Delta x} = \left| \Delta x \frac{\partial e_2^u}{\partial x} \Big|_{(0,0)} - \bar{e}_2^u \big|_* \right|, \tag{45}
$$

yields order $\mathcal{O}(\Delta x^2)$.

Consistent ghost value

Consider the numerical approximation $\bar{e}_1^s$ of the pressure $e_1^s = \frac{1}{2}(u^2 + v^2) + gs$ in the center of primal face f_1. If we assume zero external inflows to f_1, as indicated in Fig. 7, it is reasonable, to set the ghost velocities $\bar{u}_{III} = 0$ and $\bar{v}_I = 0$. Replace $U_{lef} = V_{up} = 0$, $U_{rig} = \int_0^{\frac{\Delta x}{2}} u(x, 0)\, dx$, $V_{low} = \int_{-\frac{\Delta y}{2}}^{0} v(0, y)\, dy$, and $S_{d,1} = \int_{-\frac{\Delta x}{2}}^{\frac{\Delta x}{2}} \int_{-\frac{\Delta y}{2}}^{\frac{\Delta y}{2}} s(x, y)\, dxdy$ in $\bar{e}_1^s\big|_*$. The Taylor series expansion of

$$
\epsilon_1^s = \left| \frac{\partial e_1^s}{\partial x} \Big|_{(0,0)} - \frac{1}{\Delta x} \bar{e}_1^s \big|_* \right|_{\Delta x} = \left| \Delta x \frac{\partial e_1^s}{\partial x} \Big|_{(0,0)} - \bar{e}_1^s \big|_* \right|, \tag{46}
$$

together with the zero velocity conditions $u(-\frac{\Delta x}{2}, y) = v(x, \frac{\Delta y}{2}) = 0$ on the outer boundary, yields $\epsilon_1^s = \mathcal{O}(\Delta x)$.

Inconsistent ghost value

Now consider the numerical approximation of the discharge $e_1^v = sv$ into face f_1 from below. The error

$$
\epsilon_1^v = \left| \frac{\partial e_1^v}{\partial y} \Big|_{(0,0)} - \frac{1}{\Delta y} \bar{e}_1^v \big|_* \right|_{\Delta x} = \left| \Delta x \frac{\partial e_1^u}{\partial y} \Big|_{(0,0)} - \frac{\Delta x}{\Delta y} \bar{e}_1^v \big|_* \right| \tag{47}
$$

is computed based on $S_{up} = \int_{-\frac{\Delta x}{2}}^{\frac{\Delta x}{2}} \int_0^{\Delta y} s(x, y)\, dxdy$, $V_{d,1} = \int_{-\frac{\Delta y}{2}}^{\frac{\Delta y}{2}} v(0, y)\, dy$ and $S_{low} = \Delta x \Delta y \bar{s}_I$, where $\bar{s}_I$ is the ghost value, based e. g. on the steady state. As $\bar{s}_I$ does not contain information on the actual state, the local error can be bounded only by ($f_I = [-\frac{\Delta x}{2}, \frac{\Delta x}{2}] \times [-\frac{\Delta y}{2}, 0]$)

$$
\epsilon_1^v \leq \mathcal{O}(\Delta x^2) + c \cdot \max_{(x,y) \in f_I} |v(x, y)(s(x, y) - \bar{s}_I)|. \tag{48}
$$

References

Altmann, R. and Schulze, P. (2017). A port-Hamiltonian formulation of the Navier-Stokes equations for reactive flows. *Systems & Control Letters*, 100:51–55.

Arakawa, A. and Lamb, V. R. (1981). A potential enstrophy and energy conserving scheme for the shallow water equations. *Monthly Weather Review*, 109(1):18–36.

Arnold, D., Falk, R., and Winther, R. (2010). Finite element exterior calculus: from Hodge theory to numerical stability. *Bulletin of the American Mathematical Society*, 47(2):281–354.

Arnold, V. I. (1989). *Mathematical Methods of Classical Mechanics*, volume 60. Springer.

Baaiu, A., Couenne, F., Eberard, D., Jallut, C., Lefèvre, L., Le Gorrec, Y., and Maschke, B. (2009). Port-based modelling of mass transport phenomena. *Mathematical and Computer Modelling of Dynamical Systems*, 15(3):233–254.

Brezis, H. (2011). *Functional Analysis, Sobolev Spaces and Partial Differential Equations*. Springer.

Cardoso-Ribeiro, F. L., Matignon, D., and Pommier-Budinger, V. (2017). A port-Hamiltonian model of liquid sloshing in moving containers and application to a fluid-structure system. *Journal of Fluids and Structures*, 69:402–427.

Desbrun, M., Hirani, A. N., Leok, M., and Marsden, J. E. (2005). Discrete exterior calculus. *arXiv preprint math/0508341*.

Duindam, V., Macchelli, A., Stramigioli, S., and Bruyninckx, H. (2009). *Modeling and Control of Complex Physical Systems: The Port-Hamiltonian Approach*. Springer.

Eymard, R., Gallouët, T., and Herbin, R. (2000). Finite Volume Methods. *Handbook of Numerical Analysis*, 7:713–1018.

Eymard, R. and Herbin, R. (2005). A staggered finite volume scheme on general meshes for the Navier-Stokes equations in two space dimensions. *International Journal on Finite Volumes*, 2(1):1–18.

Falaize, A. and Hélie, T. (2016). Passive guaranteed simulation of analog audio circuits: A port-Hamiltonian approach. *Applied Sciences*, 6(10):273.

Farle, O., Klis, D., Jochum, M., Floch, O., and Dyczij-Edlinger, R. (2013). A port-Hamiltonian finite-element formulation for the Maxwell equations. In *International Conference on Electromagnetics in Advanced Applications (ICEAA)*, pages 324–327. IEEE.

Flanders, H. (1963). *Differential Forms with Applications to the Physical Sciences*, volume 197. Academic Press New York.

Fornberg, B. (1990). High-order finite differences and the pseudospectral method on staggered grids. *SIAM Journal on Numerical Analysis*, 27(4):904–918.

Frankel, T. (2011). *The Geometry of Physics: an Introduction.* Cambridge University Press.

Golo, G., Talasila, V., van der Schaft, A., and Maschke, B. (2004). Hamiltonian discretization of boundary control systems. *Automatica*, 40(5):757–771.

Hiemstra, R., Toshniwal, D., Huijsmans, R., and Gerritsma, M. I. (2014). High order geometric methods with exact conservation properties. *Journal of Computational Physics*, 257:1444–1471.

Holm, D. D. (2011). *Geometric Mechanics: Dynamics and Symmetry.* Imperial College Press.

Iserles, A. (1986). Generalized leapfrog methods. *IMA Journal of Numerical Analysis*, 6(4):381–392.

Iserles, A. (2009). *A First Course in the Numerical Analysis of Differential Equations.* Number 44. Cambridge University Press.

Jänich, K. (2001). *Vector Analysis.* Springer.

Kotyczka, P. (2013). Local linear dynamics assignment in IDA-PBC. *Automatica*, 49(4):1037 − 1044.

Kotyczka, P. (2016). Finite volume structure-preserving discretization of 1D distributed-parameter port-Hamiltonian systems. *IFAC-PapersOnLine*, 49(8):298–303.

LeVeque, R. J. (2002). *Finite Volume Methods for Hyperbolic Problems*, volume 31. Cambridge University Press.

Moulla, R., Lefèvre, L., and Maschke, B. (2012). Pseudo-spectral methods for the spatial symplectic reduction of open systems of conservation laws. *Journal of Computational Physics*, 231(4):1272–1292.

Ortega, R., van der Schaft, A., Maschke, B., and Escobar, G. (2002). Interconnection and Damping Assignment Passivity-Based Control of port-controlled Hamiltonian systems. *Automatica*, 38(4):585–596.

Ortega, R., van der Schaft, A. J., Mareels, I., and Maschke, B. (2001). Putting energy back in control. *IEEE Control Syst. Mag.*, 21:18–33.

Quarteroni, A. and Valli, A. (1994). *Numerical Approximation of Partial Differential Equations.* Springer.

Seslija, M., Scherpen, J. M. A., and van der Schaft, A. J. (2014). Explicit simplicial discretization of distributed-parameter port-Hamiltonian systems. *Automatica*, 50(2):369 − 377.

Seslija, M., van der Schaft, A., and Scherpen, J. M. (2012). Discrete exterior geometry approach to structure-preserving discretization of distributed-parameter port-Hamiltonian systems. *Journal of Geometry and Physics*, 62(6):1509–1531.

Trenchant, V., Fares, Y., Ramirez, H., and Le Gorrec, Y. (2015). A port-Hamiltonian formulation of a 2D boundary controlled acoustic system. *IFAC-PapersOnLine*, 48(13):235–240.

van der Schaft, A. J. and Maschke, B. M. (2002). Hamiltonian formulation of distributed-parameter systems with boundary energy flow. *Journal of Geometry and Physics*, 42(1):166–194.

van der Schaft, A. J. and Maschke, B. M. (2011). Discrete conservation laws and port-Hamiltonian systems on graphs and complexes. *arXiv:1107.2006v1*.

van der Schaft, A. J. and Maschke, B. M. (2013). Port-Hamiltonian systems on graphs. *SIAM Journal on Control and Optimization*, 51(2):906–937.

Vu, N. M. T., Lefèvre, L., Nouailletas, R., and Brémond, S. (2017). Symplectic spatial integration schemes for systems of balance equations. *Journal of Process Control*, 51:1–17.

Warnick, K. F. and Russer, P. H. (2014). Differential forms and electromagnetic field theory. *Progress In Electromagnetics Research*, 148:83–112.

Zwart, H., Le Gorrec, Y., and Maschke, B. (2016). Building systems from simple hyperbolic ones. *Systems & Control Letters*, 91:1–6.

Bionotes

Paul Kotyczka

Paul Kotyczka is lecturer (Akademischer Rat) at the Chair of Automatic Control, Technical University of Munich. He is on a two-year research stay at University Claude Bernard Lyon 1, France, where he joined the Laboratory of Automatic Control and Chemical Engineering (LAGEP) in September 2015 as a Marie Skłodowska-Curie Fellow. Currently, he works as a postdoctoral researcher within the DFG-ANR cofunded project IN-FIDHEM. His research interests concern physical modelling, numerical methods for distributed parameter port-Hamiltonian systems and nonlinear control.

Technische Universität München, Lehrstuhl für Regelungstechnik, Boltzmannstraße 15, 85748 Garching, Germany.
kotyczka@tum.de

Bernhard Maschke

Bernhard Maschke is Professor of Automatic Control at the *Laboratory of Automatic Control and Chemical Engineering* (LAGEP UMR CNRS 5007) of the *University Claude Bernard* of Lyon, Villeurbanne, France. The main streamline of research that he developed, concerns the generalizations of Hamiltonian systems for the modelling, simulation and control of complex physical systems derived from network theory and thermodynamic theory known as *port-Hamiltonian systems*. His current research interests concern the control of port-Hamiltonian systems defined on contact manifolds, of Hamiltonian systems of conservation laws with boundary control and systems defined on graphs and k-complexes.

Univ Lyon, Université Claude Bernard Lyon 1, CNRS, LAGEP UMR 5007, 43 Boulevard du 11 Novembre 1918, 69622 Villeurbanne Cedex, France.
bernhard.maschke@univ-lyon1.fr